J Mol Model (2012) 18:2433–2442
DOI 10.1007/s00894-011-1260-8

ORIGINAL PAPER

First-principles molecular dynamics simulations of the H_2O / Cu(111) interface

Roger Nadler · Javier Fernandez Sanz

Received: 6 June 2011 / Accepted: 26 September 2011 / Published online: 18 October 2011

Abstract A first-principles theoretical study of the water-Cu(111) interface based on density functional calculations is reported. Using differently sized surface models: $p(2\times2)$, $p(4\times4)$ and $p(4\times5)$, we found out that the adsorption energy of a H_2O monomer does not significantly change with the surface model though the adsorption geometry is sensitive to the choice of the super-cell surface and, also, to the coverage. Molecular dynamics simulations on the Born-Oppenheimer surface of liquid water on a Cu(111) surface reveal that H_2O in the first solvent layer adsorbs O-down and that the H-bond network is weaker upon adsorption on the Cu. Furthermore, absolute electrochemical potentials are presented and compared to the potential of zero charge obtained experimentally and theoretically.

Keywords Condensed H2O layer · Cu(111) · H2O · H2O/Cu(111) interface · Molecular dynamics · Monomer adsorption

Introduction

A growing number of experimental and theoretical studies are performed to investigate the structure of the metal-water interface, whose ubiquity extends all over chemistry, electrochemistry, materials science, biological systems, and more. The reviews that have been written so far are rich in information about this subject [1–3] and give a complete overview about water adsorption on different metal surfaces, including low coverage adsorption, mono- and multilayer and thin water films. There is an ongoing debate about fundamental questions regarding the adsorption of water on surfaces, from isolated molecules to clusters, complete layers, and beyond.

On close-packed hexagonal metal surfaces and at low coverage, water is generally believed to form ice-like hexagonal bilayers with a $(\sqrt{3}\times\sqrt{3})R30°$ periodicity with more or less flattened rings to conform to the substrate periodicity. For instance, in the case of Ag(111) and Cu (111) surfaces, STM studies have identified the formation of cyclic water hexamers [4, 5]. However, as the experiments become more and more accurate, the classic picture of the adsorption of ice-I*h* with a $(\sqrt{3}\times\sqrt{3})R30°$ periodicity becomes questioned and different adsorption structures of the wetting layer are found. By comparing STM images of H_2O adsorbed on a Pd(111) surface with simulated STM images obtained from an optimized adsorption structure, Cerdá et al. found that the quasiperiodic $(\sqrt{3}\times\sqrt{3})R30°$ is not the unique adsorption structure [6]; the overlayers are actually formed by planar hexamer rings of nearly flat-lying water molecules. These rings then repeat to lace-like and rosette structures which also were found experimentally. On the Pt(111) surface, not only 6-, but also 5- and 7-membered rings were observed [7]. Furthermore, it was reported by Carrasco et al. that the growth of 1-D ice structure on Cu(110) surfaces occurs via pentagons [8].

Monomeric adsorption of a water molecule on metal surfaces is a difficult task, and several theoretical reports are found about this subject [9–13]. However, as different computational methods were applied, the results of the calculations may differ from one report to another. The main differences are found in the description of the adsorption geometry rather than in the quantification of the adsorption strength or the determination of the preferred adsorption position on the metal surface. While the

R. Nadler (✉) · J. F. Sanz
Dept. of Physical Chemistry, University of Seville,
41012 Seville, Spain
e-mail: rnadler@us.es

adsorption energies values reported in the aforementioned reports agree within 0.06 eV, and the preferred adsorption site for water on M(111) surfaces is always found to be the atop position, the differences in the adsorption geometries for the water monomer are significant. Fajín et al. [12] and Gokhale et al. [13] reported that the H_2O molecule lies flat on the surface without specifying more precisely the exact tilt angle, α. Tang and Chen [10] estimated α to be 8.7° while Michaelides et al. [9] found the monomer tilted away from the surface by 15°. Regarding the distance between the Cu surface atom and the O atom these reports found different results also: 2.25 Å [9], 2.36 Å [10], 2.50 and 2.54 Å [12], and finally 2.81 Å [13]. In all these commented cases the super-cell surfaces were modeled by a $p(2\times2)$ model but with different numbers of layers used. Also, different functionals and pseudopotentials were employed (see the footnotes in Table 1). Tang and Chen attributed these differences to the very flat potential energy surface of H_2O adsorption. Feibelman [14] and Vassilev et al. [15] mentioned surface size dependencies that might occur when theoretically investigating H_2O adsorption on fcc metal surfaces. Moreover, in a recent work on water-Pd(111), Poissier et al. [16] investigated the effect of the super-cell surface size of Pd(111) on the image charge distribution. They found that the surface has to be large enough in order to obtain a fully converged image charge distribution and, as a consequence, to minimize the dipole interaction between periodic images. This controversy motivated us to investigate the monomeric H_2O adsorption in the low coverage regime to try to ascertain how large a super-cell surface needs to be to obtain converged adsorption parameters. Furthermore, the adsorption geometry of a single molecule can be compared to the adsorption geometry of a H_2O molecule adsorbed from a condensed water layer.

Table 1 Adsorption parameters of water calculated for the atop site on differently sized Cu(111) surfaces and different coverage. Values from literature are tabulated as well. In Ref. [12] and [13] no absolute tilt angles are reported. The adsorption energies E_{ads} are given in eV, the tilt angles α with respect to the surface plane in degrees, and $d_{Cu\text{-}O}$ in Å. The subscript in Θ indicates the size of the super-cell surface. The bond angle is found to be 104-105° and d_{OH}=0.98 Å for all molecules

Coverage	E_{ads}	α	$d_{Cu\text{-}O}$
$\Theta_{4\times5\times7}$ =1/20	−0.18	20.8	2.33
$\Theta_{4\times4\times7}$ =1/16	−0.18	21.2	2.34
$\Theta_{4\times4\times7}$ =1/8	−0.18	13.7, 14.2	2.39
$\Theta_{4\times4\times7}$ =1/4	−0.15	0.2, 0.5, 1.1, 1.5	2.50
$\Theta_{2\times2\times7}$ =1/4	−0.13	2.1	2.84
$\Theta_{2\times2\times5,6}$ =1/4[a]	−0.24	15.1	2.25
$\Theta_{2\times2\times4}$ =1/4[b]	−0.19	8.7	2.36
$\Theta_{2\times2\times4}$ =1/4[c]	−0.22	–	–
$\Theta_{2\times2\times3}$ =1/4[d]	−0.22 (PW91)	flat	2.50
	−0.20 (PBE)		2.54
$\Theta_{2\times2\times3}$ =1/4[e]	−0.18	flat	2.81

[a] Values taken from Ref. [9]. 5 or 6 layers were used to model the slab. PW91 with US-PP

[b] Values taken from Ref. [10]. PW91 with PAW-PP were applied

[c] Values taken from Ref. [11]. PW91 and PAW-PP

[d] Values taken from Ref. [12]. PBE and PW91 with PAW-PP

[e] Values taken from Ref. [13]. The Cu slab was kept frozen. PW91 with US-PP

Dispersion effects between the metal surface atoms and the water molecules have been shown to influence energetics and structure of a given system. Using van der Waals density functional (vdW-DF) developed by Dion et al. [17], Poissier et al. obtained a larger tilt angle and a slightly larger $d_{Pd\text{-}O}$ for H_2O molecules adsorbed on Pd (111) surfaces when compared to PBE bare functional [16]. However, it was concluded that this vdW-DF approach was underperformed compared to other functionals [16]. Carrasco et al. found that dispersion is important for a general description of water-metal interactions [18] and its inclusion does better reproduce the stability of 1D and 2D wetting structure of water. However, for structure and bonding of H_2O adsorbed on metal surfaces, dispersion effects might play a minor role [18].

The connection between mono- and multimers adsorbed on a metal surface, and a system that contains a condensed H_2O layer adsorbed on the same surface is not obvious. In the latter case the properties of an adsorbed water molecule not only depends on the interaction with the underlying surface metal atom, but also on its neighbors that form the condensed water layer, *i.e.*, solvent. Certainly, the interplay between surface/adsorbate and solvent/adsorbate interactions (in the present study the solvent and adsorbate are the same) are difficult to determine, and one possible route is to compare the adsorption geometries of the H_2O monomer with those of an adsorbed water molecule surrounded by H_2O.

One of the first experimental works accounting for the metal/water interface was reported by Toney et al. [19]. They performed X-ray scattering experiments to measure the water density profile on a Ag(111) surface and found that the first solvent layer is denser compared to the bulk layer density not only for charged surfaces but also when the system is uncharged. Ataka et al. [20] analyzed the Au (111) electrode/electrolyte interface, where the electrolyte consists of perchloric acid, by means of surface-enhanced infrared absorption spectroscopy and their results support those reported by Toney et al. This issue was investigated and confirmed by means of theoretical work for various surfaces [21–24]. In these reports the density increase was found to be smaller than in experiments. Moreover, Schnur

and Gross [24] reported that the water bilayer structure is not maintained during a molecular dynamics (MD) simulation on Au(111) and Ag(111) surfaces at room temperature while on Pt(111) and Ru(0001) surfaces it was found to remain intact. These results suggest, therefore, that the structure and the density increase depend on the interaction strength between the surface metal and the adsorbed water molecules.

The strength of the H-bond network directly influences the properties of the OH bonds and the librational motion of the H_2O molecules in the bulk layer as has been shown by experiments carried out at different temperatures. Thus, Zelsmann [25] demonstrated by far IR spectroscopy that, when the temperature increases, the bands that lie below 1000 cm-1 move to lower wave numbers and are broadened. On the other end of the vibrational spectrum of water, Lock and Bakker [26] reported a temperature dependence of the symmetric and asymmetric stretch band using femtosecond mid-infrared pump-probe spectroscopy. In this case they found a blue shift of these bands as the temperature was increased. These results show how H-bond influences the vibrational structure of water and, conversely, how the IR data may be used to infer changes in the H-bond network. Intermolecular hydrogen bonds between water molecules can be comparable to or stronger than those formed between the molecule and many substrates [2, 3], and the relative strength of these two bonds determines the wetting properties of water. Hence, it is expected that the vibrational properties of water will be sensitive to the presence of a metal surface and reflect in some extension the changes in the H-bond network.

Concerning the electrochemical potential, we can start with the work of Tsiplakides et al. [27] who determined the potential of zero charge (*pzc*) for Cu on emersed rotating electrodes. In their study they also confirmed experimentally that the choice of a reference point above the emersed electrode coincides with the reference point at infinity for overall uncharged cells. From a theoretical point of view, Taylor et al. [28] developed a method to estimate the absolute electrochemical potential U_{abs} that makes use of a double reference (DR). In their procedure a single configuration of ice water structure was adopted. However, the local structure of the water layer is expected to change slightly with time, due to thermal fluctuation. Since such fluctuations might affect the potential, it seems advisable to incorporate into the model the dynamic character of the water layer in some way. Since to estimate the potential from just only one randomly selected configuration might bring unwanted instabilities, we have taken several configurations from the trajectory, and computed the potential using the DR method, omitting the geometry optimization step, the final estimation being an average of these potentials as inspired by the work of Taylor et al. [29].

In summary, in this work we report a theoretical study of the water-Cu(111) interface based on quantum mechanical calculations performed by means of density functional theory (DFT) in which some of the aforementioned points are considered. First we look at the binding energy and structure of water monomers deposited on the metal. Secondly, we perform first-principles MD simulations on the Born-Oppenheimer surface at two temperatures to obtain trajectories that will allow us to estimate the relevant interface properties such as the electrochemical potential, the planar distribution functions $g(z)$, angular probability distribution functions $p(\varphi,z)$ and $p(\theta,z)$, the water layer structure and the vibrational spectra. The analysis and comparison of the vibrational spectrum of a pure water system and the spectra obtained from the Cu-H_2O MD simulations will be of particular interest in this section.

Methods

Models

To analyze the dependence of the geometrical properties of H_2O monomers on the coverage, three slab super-cells were used to model the Cu(111) surface, namely $p(2\times2)$, $p(4\times4)$ and a $p(4\times5)$, all of them containing seven metal layers with the lowest layer kept fixed. A vacuum layer of twice the slab thickness is included. This model gives the possibility to set different coverage by adding different number of H_2O molecules: $\Theta=1/20$, 1/16, 1/8 and 1/4 ML are investigated here. This can be illustrated, for instance, by Fig. 1 where the $p(4\times4)$ super-cell is represented. With 4 H_2O adsorbed, the coverage is 1/4 ML, formally similar to

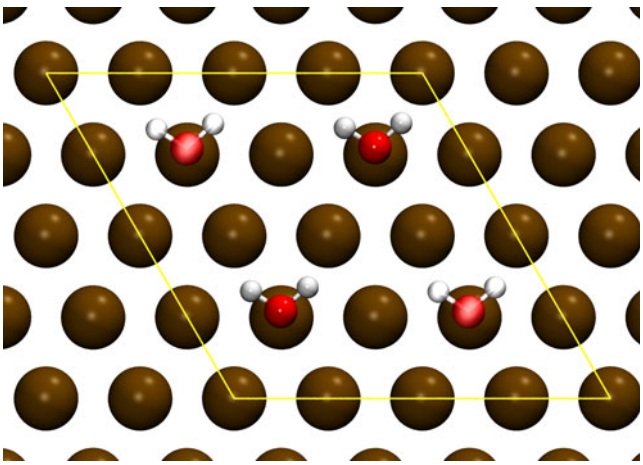

Fig. 1 The $p(4\times4)$ surface model of Cu(111), with 4 H_2O molecules on their atop adsorption position. Note that they are equivalent to four repeating units of $p(2\times2)$ surfaces. To obtain coverage of 1/8 ML the translucent molecules were removed

the models used in the literature [9–13]. If two water molecules are removed, we obtain Θ=1/8 ML (in particular, we have chosen the two translucent molecules). Finally, leaving only one water molecule we reach the coverage Θ= 1/16 ML. The adsorption energy is calculated by the formula

$$E_{\mathrm{ads}} = (E_{\mathrm{tot}} - E_{\mathrm{Cu}} - n \cdot E_{\mathrm{H2O}})/n, \quad (1)$$

where E_{tot} is the energy of the total system, E_{Cu} is the energy of the slab alone and E_{H2O} is the energy of one molecule H_2O. n is the number of water molecules adsorbed. The molecules are adsorbed on one side of the slab. Note that negative adsorption energies are equivalent to exothermic adsorption.

For the MD simulations a model consisting of a $p(3\times3)$ three-layer-thick super-cell, and a water layer was set up. This water layer is formed by 40 H_2O molecules resulting in a 23.6 Å thick solvent layer, corresponding to a water density of approximately 1.0 g · cm-3. Notice on the other hand that the equilibrium PBE density of water might not be exactly this [30], however, possible artifacts from this small difference are not expected in the region close to the solid-liquid interface [31], and actually the PBE functional has been suggested to be a good choice [16]. The middle metal slab layer was kept fixed. The MD trajectories were sampled in the canonical ensemble at a constant temperature that was controlled through the Nosé thermostat [32, 33] as implemented in VASP. This implementation does not apply velocity rescaling.

Before the Cu-water system was simulated on a first-principle level of theory, it was equilibrated using a classical force field [34, 35]. The Lorentz-Berthelot mixing rules were applied to get the Lennard-Jones parameters for the Cu-H_2O interactions. These simulations were done using the molecular mechanics driver FIST that is part of the CP2K package [36]. After a 50 ps classic run to obtain a distributed water bulk layer, the system was equilibrated at the first-principles level for 4 ps, followed by a 13 ps production run. The numerical integration was done using a time step set to 0.5 fs. On the other hand, to get a reference for pure water at the same conditions, a 20 ps MD simulation, applying a time step of 0.25 fs, of a system that contains 64 H_2O molecules in a cubic box with 12.4 Å side lengths was performed and compared to the results obtained for the Cu-H_2O systems.

Concerning the temperature of the MD simulations, it is well-known that strongly associating liquids are prone to a glassy behavior, and the range of stable liquid densities increases as the temperature is increased away from the triple point [37]. Therefore, a temperature well above the triple point is generally used. In the case of the PBE functional the proposed temperature for a correct behavior of liquid water is 330 K [30, 31], which we applied in the present work as well.

To determine the structure and orientation of H_2O in the first and second solvent layer planar distribution functions $g(z)$ and probability density functions of the angles φ and θ, $p(\varphi,z)$ and $p(\theta,z)$ were determined. In Fig. 2a graphical representation of how these angles are obtained is given. As $\mathbf{v}_{plane}$ and $\mathbf{v}_{perp}$ are perpendicular to each other, the equation

$$\theta = |90^\circ - \varphi| \quad (2)$$

holds true if the H atoms of a water molecule are located at the same height. Another relation that helps to interpret the graphs is that when the molecular plane is parallel to the surface normal, θ=90°, independently of the orientation of $\mathbf{v}_{plane}$.

Electrochemical potentials

The double reference method developed by Taylor et al. [28] gives an expression for the absolute electrochemical potential, U_{abs}, of a half cell, neutral as well as charged. To obtain U_{abs} the electrostatic potential has to be calculated by integrating the electron density over the coordinates x and y to get the electrostatic profile in the z direction. Then, two reference potentials might be introduced; one is necessary to calculate U_{abs} for neutral systems, and the second one to calculate it for charged systems. In neutral systems, the solvent layer is cleaved in the middle and a vacuum layer is introduced at this position. At this point, the first reference point will be calculated. For charged systems, a second reference point is needed. It will be calculated in the solvent layer of the charged system directly as in the charged case the electrostatic potential cannot be calculated when a vacuum is present because an electric field would occur at the interface solvent/vacuum

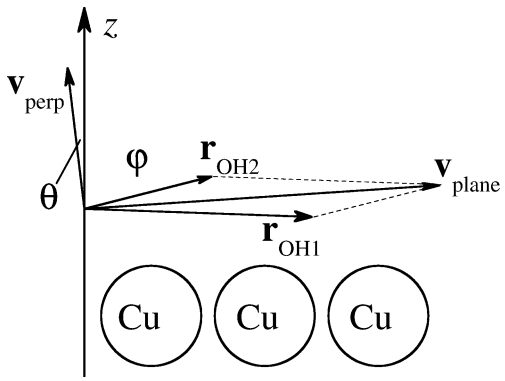

Fig. 2 In this scheme, the OH bonds of H_2O are represented by the bond vectors $\mathbf{r}_{OH1}$ and $\mathbf{r}_{OH2}$. The molecular vector $\mathbf{v}_{plane}$ is calculated as the sum of these vectors while $\mathbf{v}_{perp}$ is the vector product, so $\mathbf{v}_{plane}$ and $\mathbf{v}_{perp}$ are perpendicular to each other. φ and θ are the angles between $\mathbf{v}_{plane}$ and $\mathbf{v}_{perp}$ and the surface normal z

[28]. Here, we treated only the neutral case and U_{abs} has been calculated accordingly by

$$U_{abs} = U_{Fermi} - U_{slab,\ no\ vac} + \left(U_{slab,\ vac} - U_{ref,\ vac}\right), \qquad (3)$$

where U_{Fermi} is the Fermi potential of the system without vacuum, $U_{slab,\ no\ vac}$ is the electrostatic potential in the middle of the metal slab without vacuum, $U_{slab,\ vac}$ is the potential at the same position but with the vacuum layer present and, finally, $U_{ref,\ vac}$ is the reference point obtained by calculating the electrostatic potential in the middle of the vacuum layer. This vacuum layer should be large enough to avoid interactions between the surfaces that are introduced by cleaving the solvent layer. In the present work it was set to 15 Å.

As mentioned earlier, the procedure to calculate the absolute electrochemical potentials is slightly adapted to reflect the dynamic nature of the systems. Fifty configurations were taken out of the MD trajectory equidistantly and the electrochemical potential was directly calculated for each one, i.e., without further optimization, applying Eq. 3. The values thus obtained are averaged afterward to get a final estimate for the electrochemical potential. This adapted procedure is fairly reasonable since a measured electrochemical potential is just a time-averaged value. To reference this potential to the normal hydrogen electrode (NHE) the IUPAC recommended value of 4.44 V was used [38]:

$$U_{NHE} = -4.44 - U_{abs}. \qquad (4)$$

Computational details

Density functional calculations were carried out using the VASP code [39–41]. This code solves the Kohn-Sham equations for the valence electron density within a plane wave basis set, and makes use of the projector augmented wave (PAW) method to describe the interaction between the valence electrons and the atomic cores [42, 43]. The valence electron density is defined by the 2*s*22*p*4 electrons of each O atom, the 1*s* electron of H atom and the eleven electrons (4*s*13*d*10) of each Cu atom. The PBE functional [44] was chosen and an energy cut-off of 500 eV was set for the plane waves for the static calculations and 300 eV for the MD simulation. The Gaussian smearing method with σ=0.2 eV was used. In the static calculations the 3×2×1 set of **k**-points was used to sample the Brillouin zone of the *p*(4×4) and *p*(4×5) super-cells, and the 5×5×1 set of **k**-points for the *p*(2×2) super-cell. This setup provides a similar integration mesh density in both systems. In the MD runs, only the **Γ**-point was employed. The geometry optimizations were performed using a conjugate-gradient algorithm, which was stopped when the residual forces between the atoms were less than 1.0 · 10–2 eV/Å.

Results and discussion

Water adsorption on the Cu(111) surface

We start with the discussion of the monomeric adsorption of H_2O on the Cu(111) surface. The water-surface interaction energy has been computed using a variety of methods and models, though almost all of them make use of a *p*(2×2) super-cell of variable thickness. This model involves that the coverage is set to Θ=1/4. Also, the slab thickness used in these works was three layers [12, 13], four layers [10, 11], and five or six layers [9]. In the present study we have selectively changed the super-cell size to explore larger coverage that covers the range Θ=1/4 - 1/20. The adsorption parameters obtained using different coverage and super-cell models together with literature results are reported in Table 1. Starting with the results for $\Theta_{2\times2\times7}$=1/4, we find an adsorption energy of −0.13 eV, which is 0.05 and 0.11 eV weaker than other reported values, the differences being larger for the PW91 values. To try to explain these differences is not obvious as the calculations differ not only in the model surface but also in the functional, the pseudopotential, and in the geometry optimization conditions (number of layers fixed). The influence of the exchange correlation functional has been reported by Fajín et al. [12], who also found that the PBE adsorption energy was slightly smaller than the PW91 adsorption energy.

Let us focus now on the influence of the coverage on the Cu(111)/water surface interaction. When the coverage Θ=1/4 ML is modeled with the larger super-cell model, the *p*(4×4), the adsorption energy lowers to −0.15 eV, compared to the adsorption energy obtained from the *p*(2×2) super-cell surface. This increment in adsorption energy, although small, is accompanied by a considerable shortening of the water-surface distance by 0.34 Å and a tilt angle that is by 1° less tilted away from the surface. Although we did not consider reproducing the penta-, hexa- and heptameric structures reported earlier [6–8], we find that already for the relatively simple model presented here, H_2O is adsorbed completely flat on the metal surface for coverage of 1/4 ML.

The adsorption energies become slightly stronger when the lower coverage regime is modeled. For the three coverage values considered: 1/8, 1/16 and 1/20 ML, we find a practically identical E_{ads} of −0.18 eV, showing that the adsorption energy does not change anymore for the *p*(4×4) model with two or one water molecules adsorbed. The adsorption geometry, however, does change considerably when removing H_2O from the surface. When Θ=1/8 ML, the molecules are tilted about 13° further away from the surface than in the case of Θ=1/4 ML, going along with a reduction of the Cu-O distance by 0.11 Å. Reducing the

coverage even more (Θ=1/16 and 1/20 ML), α increases again, while the distance is shortened only a little (0.05 Å). The adsorption geometry cannot be considered as flat-lying anymore. Clearly, coverage of 1/16 ML is necessary to model purely monomeric H_2O adsorption on a Cu(111) surface. This confirms the work of Poissier et al. [16], who found the super-cell size to be an important parameter for the calculation of adsorption energies and geometries: on a small super-cell surface, the accumulated negative charge on the metal surface, induced by the adsorbed H_2O and its image neighbor, overlaps while it is completely separated when the super-cell surface is large. For $\Theta_{4\times4\times7}$=1/4 ML, neighboring water molecules have the possibility to minimize the electrostatic interactions between them, as it can be observed in Table 1. The tilt angles are different for each of the four adsorbed water molecules and vary within 1.3°. It appears that there is a delicate balance between all these factors, which actually rule the energy that imposes a geometry response to the electrostatic interaction, by moving away from the surface or by changing the tilt angle.

Structure of the H_2O/Cu(111) interface: MD simulations

To unravel the structure of the first solvent layers we start by analyzing the planar distribution functions $g_O(z)$ and $g_H(z)$ reported in the top of Fig. 3 for the upper side of the slab. Also, the position of the first and second solvent layer peaks is tabulated in Table 2. Starting with the $g_O(z)$ function, we see a first peak at 6.3 Å (2.1 Å above the Cu surface) that corresponds to the oxygen atoms of the closest water layer. This peak is followed by another intense feature in the $g_H(z)$, more than twice as high, which correspond to hydrogen atoms bound to both the first and second layer (peak at 7.2 Å) of oxygen atoms. Therefore, the water molecules are oriented with the O atom closer to the surface than the H atoms. These are located at the same distance and point away from surface into the condensed water layer. To get a clear picture, the angle probability distribution functions $p(\varphi,z)$ and $p(\theta,z)$ are analyzed and plotted in Fig. 4, and the corresponding values are tabulated in Table 2. For this first layer φ is found to be 60° and θ= 30°. By analyzing the angles with Eq. 2, the H atoms are found to be located roughly at the same height and, therefore, the molecular plane to be tilted away from the slab surface by 30°.

Table 2 Molecular angles φ and θ that determine the first solvent layer structure are assigned to its corresponding solvent layer. For each angle the center of a range is given with its limits in parenthesis. The Cu surface layer is at 4.1Å

z, [Å]	φ, [°]	θ, [°]
6.3	60 (±10)	30 (±15)
7.2	110 (±15), 160 (±10)	70 (±20)

In the second solvent layer, the molecular plane is generally found to be parallel to or slightly tilted away from the *z*-axis (70°≤θ≤80°). However, two different angles φ are found which results in two different orientations: one orientation where φ=110° and another one where φ is roughly 160º. For the first orientation, the water molecules are arranged as such that one OH bond is pointing almost perpendicular to the slab surface and the other bond has a tilt angle of around 30° away from the surface (obtained by subtracting one half of the gas phase bonding angle of water to the angle φ). This orientation is also the reason why in the top of Fig. 3 the $g_H(z)$ function of the peaks next to the surface starts at the same *z*-value as the $g_O(z)$ function. For the second orientation (φ=160°), the vector $\mathbf{v}_{plane}$ points now almost perpendicular toward the slab surface, which results in an orientation where both H atoms are closer to the surface than the O atom of the same molecule and roughly at the same height.

Concerning the intensity of the $g_O(z)$ peaks, one can see that the most intense are not the first ones but the second

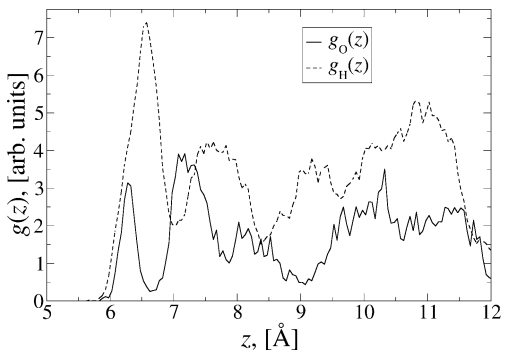

Fig. 3 Planar distribution functions *g*(*z*) of oxygen and hydrogen atoms near the surface

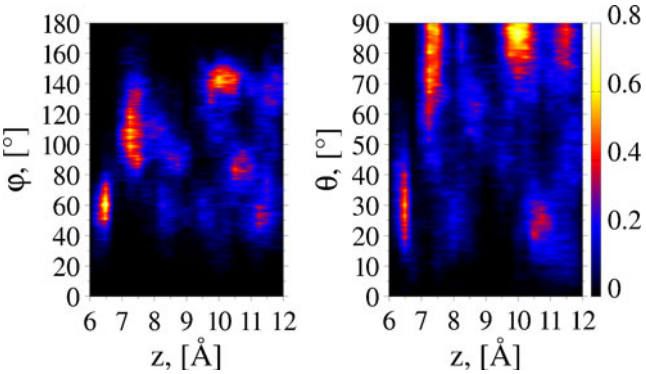

Fig. 4 Angle distribution functions $p(\varphi,z)$ and $p(\theta,z)$ of for the $Cu_{27}(H_2O)_{40}$ model. The localized probability areas near the surface indicate relatively strong metal-water interaction

peaks, which dominate over the rest of signals. This behavior indicates that the first bilayer is denser than the bulk region and is in contrast to studies of different metal surfaces where it was found that the first solvent layer is actually the densest layer [19, 21, 23, 45].

A snapshot of the adsorption structure is given in Fig. 5. At this moment, a pentagonal ring structure of water molecules has been formed on the surface as can be seen in Fig. 5a. However, the ring is distorted since the molecules forming it are located at different heights (Fig. 5b). In Fig. 5b the orientation of the first and second water layers can be nicely observed. The molecule in the first layer is oriented O-down, very similar to the adsorption geometry of the H_2O monomer at low coverage but with the molecular plane even more tilted away from the Cu surface. Although difficult to show, this increased tilt occurs most certainly upon the formation of H-bonds with the water molecule in the first solvent layer and the molecules in the second solvent layer. In this layer, H_2O has either one OH bond pointing towards the surface ($\varphi = 110°$, $\theta \approx 80°$) and, as a consequence, forming a H-bond with the underlying H_2O in the first solvent layer, which acts as the H-bond donor, or they are oriented O-up with the molecular plane approximately parallel to the *z*-axis ($\varphi = 160°$, $\theta \approx 80°$). In this case, the first solvent layer molecules are the H-bond acceptors. This snapshot is a typical structure of the first and second solvent layer as it was simulated in this work.

In earlier articles it was reported that the preferred adsorption site for H_2O monomers is atop. Also, the bridge adsorption site does show some stability compared to the hollow sites, which are the least preferred of the four possible adsorption sites (Hodgson and Haq [1] and references therein). Here, we find no different. The trajectories for the molecules that are adsorbed on the upper surface are plotted in Fig. 6. In these plots the main part of H_2O is adsorbed atop, and the movement between the atop sites takes place along the bridge sites.

The vibrational spectra of the $Cu_{27}(H_2O)_{40}$ system obtained from the MD simulations at the two temperatures are reported in Fig. 7. As may be observed the three regions of the spectrum are well delimited. There is a strong and broad band centered at around 3200 cm-1, mainly the symmetric and antisymmetric OH stretching, a well-defined peak at 1600 cm-1, corresponding to the bending modes, and the librational modes between 400 and 1000 cm-1. To compare with pure water, the spectrum obtained for the $(H_2O)_{64}$ system is also included in Fig. 7. As we can see, the bending modes lie close to each other and show equal intensities. The spectra mainly differ in that the absorption bands of the $Cu_{27}(H_2O)_{40}$ system in the 3000–3500 cm-1 region are blue-shifted by about 30 to 80 cm-1. On the other hand, the librational peaks are red-shifted by about 60 to 80 cm-1 when compared to those of the pure water system. Both shifts agree with the behavior experimentally observed [25, 26, 46]. Zelsmann [25] stated that frustrated

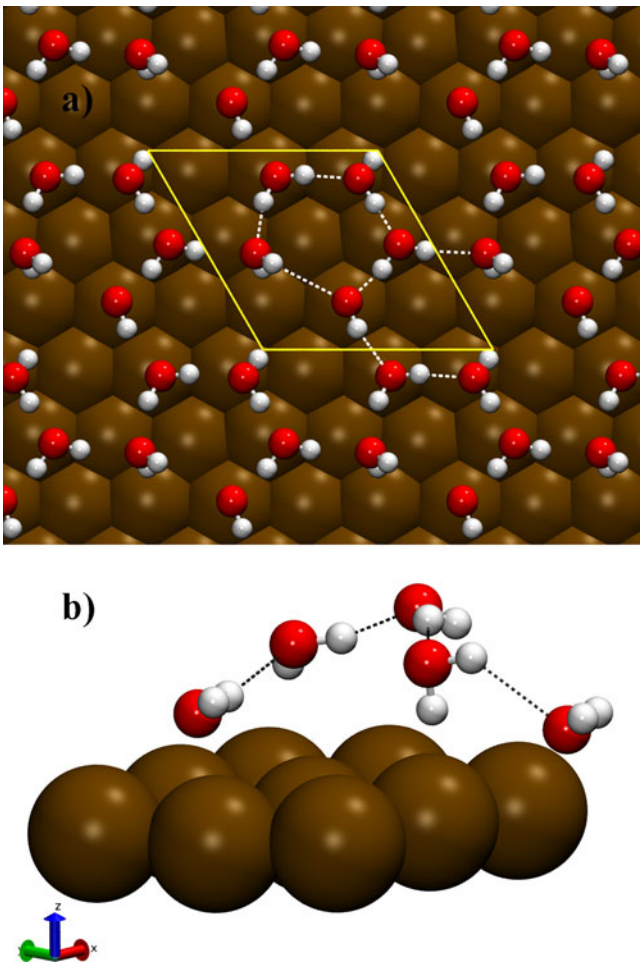

Fig. 5 A distorted pentagonal water structure is observed on the upper surface. Top (**a**) and side (**b**) views. In (**a**), the super-cell is indicated in yellow. Only the outermost Cu layer is shown in (**b**)

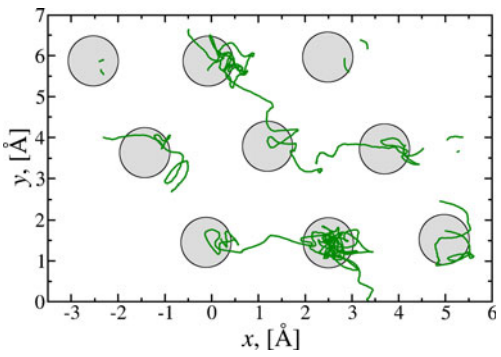

Fig. 6 Trajectories of the O atoms corresponding to the first peak closest to the upper slab surface. The lines might be discontinuous as the molecules move further away from the surface. The gray shades indicate the mean location of the corresponding Cu surface atoms

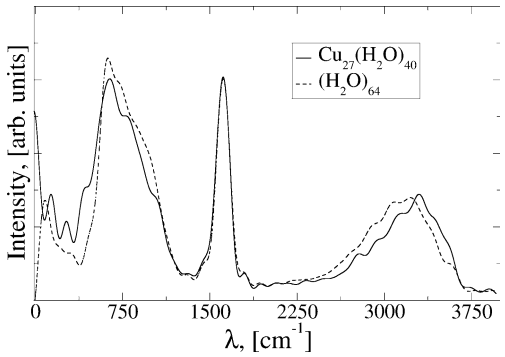

Fig. 7 Vibrational spectra of $Cu_{27}(H_2O)_{40}$ and $(H_2O)_{64}$ calculated via the velocity autocorrelation functions

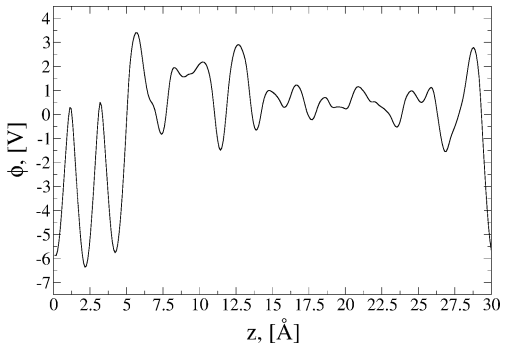

Fig. 8 Averaged electrochemical energy profile

rotation is easier to achieve at higher temperatures and, therefore, the librational modes are red-shifted, reflecting that the H-bond network is weakened. On the other hand, Lock and Bakker [26] reported a blue-shift of the stretch vibration modes at higher temperatures that they attributed to stronger OH bonds, which is consistent with a weaker H-bond network. The features observed in the present Cu-H_2O MD simulations allow us to conclude that the H-bond network weakens due to Cu-H_2O interactions.

Electrochemical potentials

Applying the modified double reference method as described above, a U_{NHE} of −0.18 ±0.59 V (U_{abs}=−4.25± 0.27 V) was obtained. This is within the range of −0.33 to −0.1 V which was reported by Clavilier and Huong [47]. Taylor et al. [28] calculated it to be 0.61 V (taking 4.44 V as reference potential instead of 4.8 V originally used in their work). This discrepancy might be attributed to the differences in the representation of the water layers. Taylor et al. used an ice structure on a face that is mirrored into the other, with the H atoms pointing into the vacuum layer directly looking at each other. This structure is quite different to the equilibrated one that we use. Moreover, as we average several configurations (50) taken from the trajectory, dynamic effects are somehow accounted for in our model. Notice on the other hand, that although the *pzc* is highly sensitive to particular experimental conditions, our value is in better agreement with the value of −0.70 eV, recently reported [48]. Moreover, the absolute electrochemical potential U_{abs} of the system presented here is similar to the work function of Cu upon water layer adsorption as well, which Tsiplakides et al. [27] have found to be −4.64 V for an emersed rotating electrode surface that corresponds to a Daniel cell and −4.80 V obtained from a 0.1 M LiOH solution. Figure 8 shows the averaged electrochemical energy profiles. The charge in the solvent layer is distributed unequally between the slab surfaces as the potential drops by roughly 0.5 V going from the left to the right.

Conclusions

In this paper we report a theoretical study of the structure of a water layer interacting with a Cu surface, based on MD simulations performed using DF calculations. Using a double reference method and a set of configurations extracted from the trajectory we have estimated an electrochemical potential of −0.18 V (NHE).

The adsorption energies, E_{ads}, and the tilt angle α of water monomers on the Cu(111) surface are sensitive measures and vary strongly with the coverage. Neighboring H_2O molecules do interact electrostatically with each other and change the Cu-H_2O interaction kind. As coverage is 1/4 ML, the water molecules are adsorbed almost parallel to the surface and the Cu-O distance is largest for the larger super-cell surface $p(4\times4)$. This is consistent with experimental reports where H_2O is found to adsorb flatly on the metal surface in the sub-monolayer regime [6, 7]. As far as coverage is concerned, our calculations using a $p(4\times4)$ 7-layer-thick super-cell show that the energy does not change further when Θ=1/8 ML, while the geometrical adsorption parameters $d_{Cu\text{-}O}$ and α obtain their monomeric geometry at Θ=1/16 ML, which is, therefore, the coverage that will reproduce the purely monomeric water adsorption on the Cu(111) surface.

Analysis of the angles φ and θ reveals that in the first solvent layer the molecules are mainly arranged in an O-down orientation and with their molecular plane tilted away from the metal surface, which is similar to the adsorption geometry of the H_2O monomer at low coverage. The preferred site for adsorption is on top of the Cu surface atoms. In the second solvent layer the molecular planes are nearly parallel to the *z*-axis and one or two OH-bonds point toward the surface.

The presence of the Cu surface alters the H-bond network. The effects are similar to those observed when the temperature of a pure water system is increased. The H-bond network weakens and the OH bonds become stronger which is reflected by a red-shift of the librational modes and a blue-shift of the symmetric and asymmetric stretching vibration modes.

Acknowledgments This work was funded by the Spanish Ministerio de Ciencia e Innovación, MICINN, projects MAT2008-4918 and CSD2008-0023. RN thanks the Junta de Andalucía for a pre-doctoral grant (P08-FQM-3661). Part of the calculations has been carried out at the Barcelona Supercomputing Center -Centro Nacional de Supercomputación (Spain).

References

1. Hodgson A, Haq S (2009) Water adsorption and the wetting of metal surfaces. Surf Sci Rep 64:381–451. doi:10.1016/j.surfrep.2009.07.001
2. Henderson M (2002) The interaction of water with solid surfaces: Fundamental aspects revisited. Surf Sci Rep 46:1–308. doi:10.1016/S0167-5729(01)00020-6
3. Thiel P, Madey T (1987) The interaction of water with solid surfaces: Fundamental aspects. Surf Sci Rep 7:211–385. doi:10.1016/0167-5729(87)90001-X
4. Morgenstern K, Nieminen J (2002) Intermolecular bond length of ice on Ag(111). Phys Rev Lett 88:066102. doi:10.1103/PhysRevLett.88.066102
5. Morgenstern K, Rieder K (2002) Formation of the cyclic ice hexamer via excitation of vibrational molecular modes by the scanning tunneling microscope. J Chem Phys 116:5746–5753. doi:10.1063/1.1453965
6. Cerdá J, Michaelides A, Bocquet M, Feibelman P, Mitsui T, Rose M, Fomin E, Salmeron M (2010) Novel water overlayer growth on Pd(111) characterized with scanning tunneling microscopy and density functional theory. Phys Rev Lett 93:116101. doi:10.1103/PhysRevLett.93.116101
7. Nie S, Feibelman P, Bartelt N, Thürmer K (2010) Pentagons and heptagons in the first water layer on Pt(111). Phys Rev Lett 105:026102. doi:10.1103/PhysRevLett.105.026102
8. Carrasco J, Michaelides A, Forster M, Haq S, Raval R, Hodgson A (2009) A one-dimensional ice structure built from pentagons. Nat Mater 8:427–431. doi:10.1038/nmat2403
9. Michaelides A, Ranea V, De Andres P, King D (2003) General model for water monomer adsorption on close-packed transition and noble metal surfaces. Phys Rev Lett 90:216102. doi:10.1103/PhysRevLett.90.216102
10. Tang Q, Chen Z (2007) Density functional slab model studies of water adsorption on flat and stepped Cu surfaces. Surf Sci 601:954–964. doi:10.1016/j.susc.2006.11.036
11. Wang G, Nakamura J (2010) Structure sensitivity for forward and reverse water-gas shift reactions on copper surfaces: a DFT study. J Phys Chem Lett 1:3053–3057. doi:10.1021/jz101150w
12. Fajín J, Illas F, Gomes J (2009) Effect of the exchange-correlation potential and of surface relaxation on the description of the H2O dissociation on Cu(111). J Chem Phys 130:224702–224710. doi:10.1063/1.3149851
13. Gokhale A, Dumesic J, Mavrikakis M (2008) On the mechanism of low-temperature water gas shift reaction on copper. J Am Chem Soc 130:1402–1414. doi:10.1021/ja0768237
14. Feibelman P (2002) Partial dissociation of water on Ru(0001). Science 295:99–102. doi:10.1126/science.1065483
15. Vassilev P, van Santen R, Koper M (2005) *Ab initio* studies of a water layer at transition metal surfaces. J Chem Phys 122:054701–054713. doi:10.1063/1.1834489
16. Poissier A, Ganeshan S, Fernández-Serra M (2011) The role of hydrogen bonding in water–metal interactions. Phys Chem Chem Phys 13:3375–3384. doi:10.1039/C0CP00994F
17. Dion M, Rydberg H, Schröder E, Langreth D, Lundqvist B (2004) Van der Waals density functional for general geometries. Phys Rev Lett 92:246401–246405. doi:10.1103/PhysRevLett.92.246401
18. Carrasco J, Santra B, Klimeš J, Michaelides A (2011) To wet or not to wet? Dispersion forces tip the balance for water ice on metals. Phys Rev Lett 106:026101–026105. doi:10.1103/PhysRevLett.106.026101
19. Toney M, Howard J, Richer J, Borges G, Gordon J, Melroy O, Wiesler D, Yee D, Sorensen L (1994) Voltage-dependent ordering of water molecules at an electrode–electrolyte interface. Nature 368:444–446. doi:10.1038/368444a0
20. Ataka K, Yotsuyanagi T, Osawa M (1996) Potential-dependent reorientation of water molecules at an electrode/electrolyte interface studied by surface-enhanced infrared absorption spectroscopy. J Phys Chem 100:10664
21. Price D, Halley J (1995) Molecular dynamics, density functional theory of the metal–electrolyte interface. J Chem Phys 102:6603–6613. doi:10.1063/1.469376
22. Izvekov S, Mazzolo A, VanOpdorp K, Voth G (2001) *Ab initio* molecular dynamics simulation of the Cu(110)–water interface. J Chem Phys 114:3248–3258. doi:10.1063/1.1342859
23. Izvekov S, Voth G (2001) *Ab initio* molecular dynamics simulation of the Ag(111)-water interface. J Chem Phys 115:7196–7207. doi:10.1063/1.1403438
24. Schnur S, Gross A (2009) Properties of metal–water interfaces studied from first principles. New J Phys 11:125003. doi:10.1088/1367-2630/11/12/125003
25. Zelsmann H (1995) Temperature dependence of the optical constants for liquid H2O and D2O in the far IR region. J Mol Struct 350:95–114. doi:10.1016/0022-2860(94)08471-S
26. Lock A, Bakker H (2002) Temperature dependence of vibrational relaxation in liquid H2O. J Chem Phys 117:1708–1714. doi:10.1063/1.1485966
27. Tsiplakides D, Archonta D, Vayenas C (2007) Absolute potential measurements in solid and aqueous electrochemistry using two Kelvin probes and their implications for the electrochemical promotion of catalysis. Top Catal 44:469–479. doi:10.1007/s11244-006-0139-x
28. Taylor C, Wasileski S, Filhol J, Neurock M (2006) First principles reaction modeling of the electrochemical interface: Consideration and calculation of a tunable surface potential from atomic and electronic structure. Phys Rev B 73:165402. doi:10.1103/PhysRevB.73.165402
29. Taylor C, Kelly R, Neurock M (2006) First Principles Modeling of Structure and Reactivity at the Metal/Water Interface. Dissertation, University of Virginia
30. McGrath M, Siepmann J, Kuo I, Mundy C (2006) Vapor-liquid equilibria of water from first principles: comparison of density functionals and basis sets. Mol Phys 104:3619–3626. doi:10.1080/00268970601014781
31. Liu L, Krack M, Michaelides A (2009) Interfacial water: A first principles molecular dynamics study of a nanoscale water film on salt. J Chem Phys 130:234702–234714. doi:10.1063/1.3152845
32. Nosé S (1984) A unified formulation of the constant temperature molecular dynamics methods. J Chem Phys 81:511–520. doi:10.1063/1.447334
33. Nosé S (1984) A molecular dynamics method for simulations in the canonical ensemble. Mol Phys 52:255–268. doi:10.1080/00268978400101201
34. Zhang X, Liu Q, Zhu A (2007) An improved fully flexible fixed-point charges model for water from ambient to supercritical condition. Fluid Phase Equilib 262:210–216. doi:10.1016/j.fluid.2007.09.005
35. Heinz H, Vaia R, Farmer B, Naik R (2008) Accurate simulation of surfaces and interfaces of face-centered cubic metals using 12–6 and 9–6 Lennard-Jones potentials. J Phys Chem C 112:17281–17290. doi:10.1021/jp801931d
36. CP2K Developers Home Page http://cp2k.berlios.de.
37. Hansen J, McDonald I (1986) Theory of simple liquids, 2nd edn. Academic, New York

38. Trasatti S (1986) The absolute electrode potential: an explanatory note. Pure Appl Chem 58:955–966. doi:10.1351/pac198658070955S
39. Kresse G, Hafner J (1993) *Ab initio* molecular dynamics for liquid metals. Phys Rev B 47:558–561. doi:10.1103/PhysRevB.47.558
40. Kresse G, Furthmüller J (1996) Efficiency of ab-initio total energy calculations for metals and semiconductors using a plane-wave basis set. Comput Mater Sci 6:15–50. doi:10.1016/0927-0256(96)00008-0
41. Kresse G, Furthmüller J (1996) Efficient iterative schemes for *ab initio* total-energy calculations using a plane-wave basis set. Phys Rev B 54:11169–11186. doi:10.1103/PhysRevB.54.11169
42. Blöchl P (1994) Projector augmented-wave method. Phys Rev B 50:17953–17979. doi:10.1103/PhysRevB.50.17953
43. Kresse G, Joubert D (1999) From ultrasoft pseudopotentials to the projector augmented-wave method. Phys Rev B 59:1758–1775. doi:10.1103/PhysRevB.59.1758
44. Perdew J, Burke K, Ernzerhof M (1996) Generalized gradient approximation made simple. Phys Rev Lett 77:3865–3868. doi:10.1103/PhysRevLett.77.3865
45. Otani M, Hamada I, Sugino O, Morikawa Y, Okamoto Y, Ikeshoji T (2008) Structure of the water/platinum interface—a first principles simulation under bias potential. Phys Chem Chem Phys 10:3609–3612. doi:10.1039/B803541E
46. Miura N, Yamada H, Moon A (2010) Intermolecular vibrational study in liquid water and ice by using far infrared spectroscopy with synchrotron radiation of MIRRORCLE 20. Spectrochimica Acta Part A 77:1048–1053. doi:10.1016/j.saa.2010.08.071
47. Clavilier J, Huong C (1969) Compt Rend Ser C 269:736
48. Walbran S, Mazzolo A, Halley J, Price D (1998) Model for the electrostatic response of the copper–water interface. J Chem Phys 109:8076–8081. doi:10.1063/1.477455